Measurement of the invariant-mass spectrum for the two photons from the $\eta \to \pi^0\gamma\gamma$ decay

S. Prakhov,[1] B. M. K. Nefkens,[1] C. E. Allgower,[2,*] V. Bekrenev,[3] W. J. Briscoe,[4] J. R. Comfort,[5] K. Craig,[5] D. Grosnick,[6] D. Isenhower,[7] N. Knecht,[8,†] D. Koetke,[6] A. Koulbardis,[3] N. Kozlenko,[3] S. Kruglov,[3] G. Lolos,[8] I. Lopatin,[3] D. M. Manley,[9] R. Manweiler,[6] A. Marušić,[1,‡] S. McDonald,[1,§] J. Olmsted,[1,‖] Z. Papandreou,[8] D. Peaslee,[10] N. Phaisangittisakul,[1] J. W. Price,[1] A. F. Ramirez,[5] M. Sadler,[7] A. Shafi,[4] H. Spinka,[2] T. D. S. Stanislaus,[6] A. Starostin,[1] H. M. Staudenmaier,[11] and I. Supek[12]
(Crystal Ball Collaboration at the AGS)
[1]*University of California Los Angeles, Los Angeles, California 90095-1547, USA*
[2]*Argonne National Laboratory, Argonne, Illinois 60439-4815, USA*
[3]*Petersburg Nuclear Physics Institute, Gatchina RU-188350, Russia*
[4]*The George Washington University, Washington, D.C. 20052-0001, USA*
[5]*Arizona State University, Tempe, Arizona 85287-1504, USA*
[6]*Valparaiso University, Valparaiso, Indiana 46383-6493, USA*
[7]*Abilene Christian University, Abilene, Texas 79699-7963, USA*
[8]*University of Regina, Saskatchewan, Canada, S4S OA2*
[9]*Kent State University, Kent, Ohio 44242-0001, USA*
[10]*University of Maryland, College Park, Maryland 20742-4111, USA*
[11]*Universität Karlsruhe, Karlsruhe D-76128, Germany*
[12]*Rudjer Boskovic Institute, Zagreb 10002, Croatia*
(Received 21 March 2008; published 24 July 2008)

New results on the rare, doubly radiative decay $\eta \to \pi^0\gamma\gamma$ have been obtained from a revised analysis of the Crystal Ball experiment performed at the AGS. The analysis yields the first information on the dependence of the decay width, $\Gamma(\eta \to \pi^0\gamma\gamma)$, on the two-photon invariant mass squared, $m^2(\gamma\gamma)$. A re-evaluation of the branching ratio is also made, $BR(\eta \to \pi^0\gamma\gamma) = (2.21 \pm 0.24_{\text{stat}} \pm 0.47_{\text{syst}}) \times 10^{-4}$; it implies that the decay width is $\Gamma(\eta \to \pi^0\gamma\gamma) = 0.285 \pm 0.031_{\text{stat}} \pm 0.061_{\text{syst}}$ eV. These results are close to predictions based on chiral perturbation theory with vector-meson dominance.

DOI: 10.1103/PhysRevC.78.015206 PACS number(s): 14.40.Aq, 13.20.−v, 12.39.Fe

I. INTRODUCTION

The rare, doubly radiative decay

$$\eta \to \pi^0\gamma\gamma \tag{1}$$

has attracted much attention as there are large uncertainties in the experimental determination of its decay width and in the calculations based on chiral perturbation theory (χPTh), which uses a momentum expansion and typically provides a good description of the strong and electroweak interactions of pseudoscalar mesons at low energies [1]. The uncertainties in χPTh calculations of the amplitude for the $\eta \to \pi^0\gamma\gamma$ transition are related to the fact that the lowest order lagrangian of χPTh [order two in particle four-momentum or masses, $\mathcal{O}(\mathsf{p}^2)$] and the tree contributions at $\mathcal{O}(\mathsf{p}^4)$ are zero as neither π^0 nor η can emit a photon. The pion and kaon loops at $\mathcal{O}(\mathsf{p}^4)$ are greatly suppressed due to, respectively, G-parity invariance and the large mass of the kaons. The main contribution to the $\eta \to \pi^0\gamma\gamma$ decay amplitude comes from the $\mathcal{O}(\mathsf{p}^6)$ counterterms that are needed in χPTh to cancel various divergences. The coefficients of these counterterms are not determined by χPTh itself; they depend on the model used for the calculation. As the $\eta \to \pi^0\gamma\gamma$ decay has a three-body final state, its Dalitz plot reflects the decay amplitude. Thus, a complete test of χPTh with its $\mathcal{O}(\mathsf{p}^6)$ chiral coefficients requires an experimental measurement of both the $\eta \to \pi^0\gamma\gamma$ decay rate and the Dalitz plot. So far this has not been done.

The experimental challenges of measuring $\eta \to \pi^0\gamma\gamma \to 4\gamma$ are formidable because of the smallness of the rate for doubly radiative decays, which is expected to be smaller than for strong decays by a factor of order $\alpha^2 \approx 1/137^2$. In practice, it requires the suppression of large backgrounds and the subtraction of the remaining background contributions. Major backgrounds, which can mimic $\eta \to \pi^0\gamma\gamma$ events, come from $\eta \to 3\pi^0 \to 6\gamma$ decays with electromagnetic showers that overlap in the photon detector and also from $\eta \to \gamma\gamma$ decays with split-off showers. As $BR(\eta \to 3\pi^0) = 0.325$ and $BR(\eta \to \gamma\gamma) = 0.394$, the background from these η decay modes is usually significant for all types of photon detectors. In the experiments where η mesons are produced from the decay of baryon resonances, the largest contribution to the four-photon final state comes from $\pi^0\pi^0$ production. Therefore, this process must be suppressed substantially during the analysis in order to see the tiny signal from $\eta \to \pi^0\gamma\gamma$. This is even more important for a measurement of the $\eta \to \pi^0\gamma\gamma$ Dalitz

*Present address: Midwest Proton Radiotherapy Institute, 2425 Milo B. Sampson Ln., Bloomington, IN 47408, USA.
†Present address: Physics Dept. of University of Toronto, 60 St. George St., Toronto, Ontario, Canada, M5S 1A7.
‡Present address: Collider-Accelerator Dept., Brookhaven National Laboratory, Upton, NY 11973, USA.
§Present address: TRIUMF, 4004 Wesbrook Mall, Vancouver, B.C., Canada, V6T 2A3.
‖Present address: Lancaster General Hospital, Radiation Oncology, Lancaster, PA 17604, USA.

plot needed for understanding the decay amplitude. Since the density of the event distribution across the $\eta \to \pi^0\gamma\gamma$ Dalitz plot varies depending on the model used in the χPTh calculations, a good experimental acceptance for the full Dalitz plot is also essential.

The history of early attempts to measure and calculate the $\eta \to \pi^0\gamma\gamma$ decay have been reviewed in detail in Ref. [2]. A major advance was made in 1981 with the GAMS experiment [3,4], which used a forward wall of 1400 Cerenkov counters that provided good energy and spatial resolution for high-energy photons. A total of $6 \times 10^5 \eta$ mesons were produced in the $\pi^- p \to \eta n$ reaction, improving the statistics compared to previous experiments by two orders of magnitude. A narrow peak of 40 events in the $\pi^0\gamma\gamma$ invariant-mass spectrum at the mass of the η meson was interpreted as the $\eta \to \pi^0\gamma\gamma$ signal. Much attention was paid to suppressing the $\eta \to 3\pi^0$ background. In 1982, the GAMS collaboration reported that $BR(\eta \to \pi^0\gamma\gamma) = (9.5 \pm 2.3) \times 10^{-4}$ [3]. A better understanding of the $\eta \to 3\pi^0$ background resulted in a smaller value, $BR(\eta \to \pi^0\gamma\gamma) = (7.1 \pm 1.4) \times 10^{-4}$, published in 1984 [4]. No estimate of the remaining $\eta \to 3\pi^0$ background among the $\eta \to \pi^0\gamma\gamma$ candidates was presented.

For two decades, the revised GAMS result, $\Gamma(\eta \to \pi^0\gamma\gamma) = 0.84 \pm 0.17$ eV [4], was the favored experimental value for this decay width. It brought much interest to theoretical calculations that tried to reproduce the surprisingly large $\eta \to \pi^0\gamma\gamma$ decay width. According to Ametller *et al.* [5], the decay amplitude based only on vector-meson dominance (VMD) yields $\Gamma(\eta \to \pi^0\gamma\gamma) = 0.31$ eV. Including the pion and kaon loops at $\mathcal{O}(\mathrm{p}^4)$ and $\mathcal{O}(\mathrm{p}^8)$ increases the width to 0.42 eV. Finally, adding a_0- and a_2-meson exchange, with the assumption of constructive interference with vector mesons, results in a width of 0.50 eV. This is only about half the experimental value for $\Gamma(\eta \to \pi^0\gamma\gamma)$. Similar VMD results have been obtained by Ng and Peters [6]: $\Gamma_{\mathrm{VMD}}(\eta \to \pi^0\gamma\gamma) = 0.30^{+0.16}_{-0.13}$ eV and $\Gamma_{\mathrm{VMD}+a_0}(\eta \to \pi^0\gamma\gamma) = 0.37^{+0.23}_{-0.17}$ eV. The same authors increase the predicted $\eta \to \pi^0\gamma\gamma$ decay width to 0.70 eV in a study based on the quark-box diagram [7]. Ko in Ref. [8] revised the calculation of Ref. [5] by including contributions of C-odd axial-vector resonances; his result is $\Gamma(\eta \to \pi^0\gamma\gamma) = 0.47 \pm 0.20$ eV. Jetter in Ref. [9], using two different models, obtained $\Gamma_{L^6+\mathcal{O}(\mathrm{p}^4)+L^4+\mathrm{fact.}}(\eta \to \pi^0\gamma\gamma) = 0.77 \pm 0.16$ eV and $\Gamma_{\mathrm{VMD+loops}}(\eta \to \pi^0\gamma\gamma) = 0.44 \pm 0.09$ eV. The study of the $\eta \to \pi^0\gamma\gamma$ decay via the quark-box diagram in the three-flavor Nambu-Jona-Lasinio model by Nemoto *et al.* [10] resulted in 0.92 eV for the decay width. From the overview of the existing calculations, one can see that only the calculations based on the quark-box diagram get close to the GAMS result for $\Gamma(\eta \to \pi^0\gamma\gamma)$.

After 2001, the experimental situation on measuring the $\eta \to \pi^0\gamma\gamma$ decay changed greatly. New experiments reported decay-width values that were two to three times smaller than the GAMS result and were in better agreement with χPTh calculations. The Crystal Ball (CB) collaboration at the AGS conducted an experiment devoted to investigations of rare η-meson decays with a total of 2.8×10^7 η mesons produced in the $\pi^- p \to \eta n$ reaction near threshold. Our analysis of these data [11,12,14] resulted in $BR(\eta \to \pi^0\gamma\gamma) = (3.5 \pm 0.7_{\mathrm{stat}} \pm 0.6_{\mathrm{syst}}) \times 10^{-4}$. An independent analysis [13] of the same CB data yielded the relative branching ratio $B_1 = (8.3 \pm 2.8_{\mathrm{stat}} \pm 1.4_{\mathrm{syst}}) \times 10^{-4}$ with respect to $BR(\eta \to 3\pi^0)$; this implies $BR(\eta \to \pi^0\gamma\gamma) = (2.7 \pm 0.9_{\mathrm{stat}} \pm 0.5_{\mathrm{syst}}) \times 10^{-4}$. Meanwhile, the SND collaboration at VEPP-2M reported $BR(\eta \to \pi^0\gamma\gamma) = (2.1^{+3.8}_{-1.9}) \times 10^{-4}$ [2]. However, the signal was just $7.0^{+12.9}_{-6.5}$ events.

The most recent χPTh calculations of $\Gamma(\eta \to \pi^0\gamma\gamma)$, which revised earlier ones, resulted in 0.47 ± 0.10 eV [15] and 0.45—0.53 eV [16], showing good agreement with the latest experimental values, like $\Gamma(\eta \to \pi^0\gamma\gamma) = 0.45 \pm 0.12$ eV from Ref. [14]. Surprisingly low in comparison with all earlier measurements and χPTh calculations, is the recent result of the KLOE collaboration [17], $BR(\eta \to \pi^0\gamma\gamma) = (0.84 \pm 0.27_{\mathrm{stat}} \pm 0.14_{\mathrm{syst}}) \times 10^{-4}$ which is based on a signal of 68 ± 23 events. From the theoretical point of view, a small decay width like this could be the result of destructive interference between the vector-meson and other meson contributions. To check this hypothesis experimentally, one must investigate the density of the $\eta \to \pi^0\gamma\gamma$ Dalitz plot, which reflects the decay amplitude. A smaller value for $BR(\eta \to \pi^0\gamma\gamma)$ could also be obtained if the KLOE detection efficiency depends much on the $\eta \to \pi^0\gamma\gamma$ decay amplitude.

One can see that the existing experimental results and theoretical calculations for $\Gamma(\eta \to \pi^0\gamma\gamma)$ vary a lot. Also, strictly speaking, the agreement between the measured and calculated decay width is not sufficient to prove χPTh calculations. Since every calculation of $\Gamma(\eta \to \pi^0\gamma\gamma)$ makes a specific prediction for the decay Dalitz plot, the experimental measurement of this plot must also confirm the theoretical prediction. Instead of a Dalitz plot, χPTh calculations usually depict the $d\Gamma(\eta \to \pi^0\gamma\gamma)$ dependence on the two-photon invariant mass, $m(\gamma\gamma)$, [or the invariant mass squared, $m^2(\gamma\gamma)$] in the $\eta \to \pi^0\gamma\gamma$ decay. In Fig. 1, we illustrate the predictions for both the $m(\gamma\gamma)$ and $m^2(\gamma\gamma)$ spectra, which are obtained from the decay amplitudes described in detail in Refs. [6,7]. The prediction based on the vector-meson contribution alone gives the basic decay width and two-photon invariant-mass spectrum that is close to phase space in the region where $m^2(\gamma\gamma) > 0.05$ GeV$^2/c^4$. Note that the "pure" VMD prediction for $d\Gamma(\eta \to \pi^0\gamma\gamma)/dm(\gamma\gamma)$ is similar for most of the existing calculations [5,6,8,9,15]. Adding other contributions to the vector-meson part, for example a_0-meson exchange, changes the decay width and the invariant-mass spectrum, which depend on the sign of the interference term. As shown in Fig. 1, there is a typical correlation between the change of the decay width and the change in the two-photon invariant-mass spectrum. Evidently, increasing the total decay width occurs mostly due to the rise in the $d\Gamma(\eta \to \pi^0\gamma\gamma)$ spectrum at high $m(\gamma\gamma)$ values.

Thus far none of the experiments has presented a reliable measurement of the $\gamma\gamma$ invariant-mass spectrum, which is needed to provide a unique test of χPTh calculations and to obtain the information necessary for determining the coefficients of the $\mathcal{O}(\mathrm{p}^6)$ counterterms.

In this paper, we present the first results for the $d\Gamma(\eta \to \pi^0\gamma\gamma)/dm^2(\gamma\gamma)$ distribution and a new value for the $\eta \to$

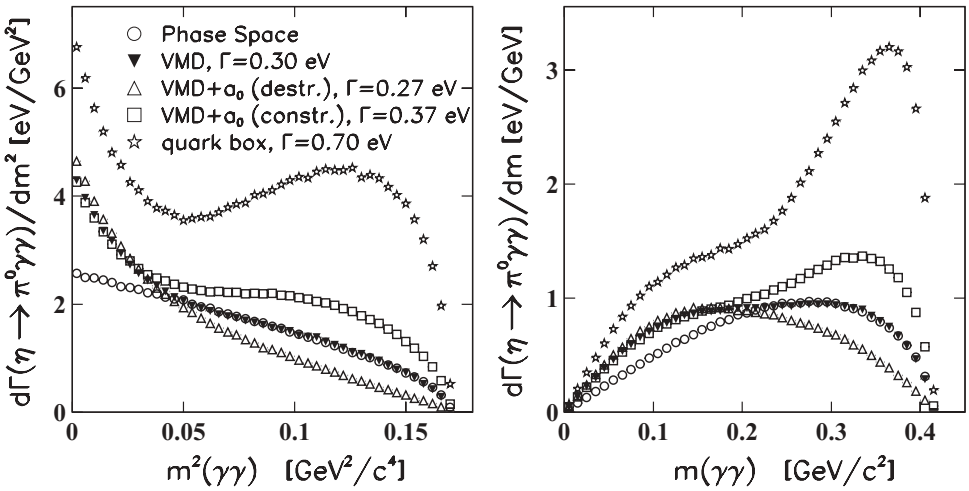

FIG. 1. Comparison of the χPTh calculations of Refs. [6,7] showing the dependence of the $\eta \to \pi^0\gamma\gamma$ decay width on $m^2(\gamma\gamma)$ (left) and on $m(\gamma\gamma)$ (right).

$\pi^0\gamma\gamma$ branching ratio, where both are obtained from an expanded analysis of the Crystal Ball experiment performed at the AGS. We omit many experimental details that have already been presented in Ref. [14]. We will mostly focus on the optimization of our selection criteria, which enable us to have a good acceptance and small background for the $\eta \to \pi^0\gamma\gamma$ Dalitz plot, and on the use of a new fitting procedure for the experimental $m(\pi^0\gamma\gamma)$ spectra.

II. EXPERIMENTAL ARRANGEMENTS

The experiment was performed with the Crystal Ball multiphoton spectrometer, which consists of 672 optically isolated NaI(Tl) crystals arranged in two hemispheres that cover 93% of 4π sr. More details about the CB detector at the AGS and the analyses of its data can be found in Refs. [13,18–21]. Details of the present experiment have been given in Ref. [14]; here we review the most important ones.

The experiment used a momentum-analyzed beam of negative pions incident on a 10-cm-long liquid hydrogen (LH_2) target located in the center of the CB. The mean value of the incident momentum spectrum at the center of the LH_2 target was 716 MeV/c (that is just above the $\pi^- p \to \eta n$ threshold), the momentum spread was $\sim$ 12 MeV/c, and the momentum resolution of an individual beam particle was $\sim$ 0.6%.

The number of $\pi^- p \to \eta n$ events produced in our experiment, 2.8×10^7, was determined using the $\eta \to \gamma\gamma$ decay mode. The quality of the data analysis and Monte Carlo (MC) simulation is shown in Ref. [14], which illustrates the agreement between the data and the MC distributions obtained for the sequential processes $\pi^- p \to \eta n \to \gamma\gamma n$ and $\pi^- p \to \eta n \to 3\pi^0 n \to 6\gamma n$.

A "cluster" in the CB was defined as a group of neighboring crystals in which energy was deposited from the electromagnetic shower of a single photon. The software threshold for the cluster energy was chosen to be 14 MeV; this optimizes the number of the reconstructed $\pi^- p \to \eta n$ events for η decaying in all neutral modes.

In our analysis, all clusters in the CB were assumed to be produced by the electromagnetic showers of the final-state photons. The neutron was analyzed as the missing particle. Since the $\pi^- p \to \eta n$ reaction was explored near the production threshold when the majority of the final-state neutrons leave through the downstream tunnel of the CB, the fraction of η events with the neutron detected in the CB is only 5%. Therefore, we neglected in our analysis the events in which there was an extra cluster from a neutron interaction in the CB.

As the decay time of NaI(Tl) is about 250 ns, the high intensity of the incident pion beam causes good events to be contaminated by so-called pile-up clusters (i.e., remaining clusters from other events). If the original cluster multiplicity of good events is changed because of the pile-up clusters, those events can be lost for the analysis. Elimination of the pile-up clusters was based on the TDC information of the crystals forming the clusters. All clusters that occur outside the proper TDC gate were eliminated from further consideration. However, the efficiency of this procedure depends on the cluster energy. Because of the hardware thresholds, many clusters with energy below 40 MeV have no TDC information, which does not enable us to distinguish between the good and pile-up clusters. In our analysis, the events contaminated with low-energy pile-up clusters were eliminated by the same cut that was used to suppress the $\eta \to \gamma\gamma$ background with split-off showers. This cut rejected all events having clusters with energy larger than 40 MeV; see next section for more details.

In the MC simulation of $\pi^- p \to \eta n$, we used the beam spectrum obtained for η events from the experimental data. The production angular distribution for $\pi^- p \to \eta n$ needed in the MC simulation was also determined from the data. The simulation of the $\eta \to 3\pi^0$ decay was made according to phase space. The simulation of the $\eta \to \pi^0\gamma\gamma$ decay was made according to the decay amplitudes from Ref. [6] and also according to phase space. The MC events were propagated through a full GEANT (version 3.21) simulation of the CB detector, folded with the CB resolutions and trigger conditions, and analyzed the same way as the experimental data.

III. SELECTION OF THE $\pi^- p \to \pi^0\gamma\gamma n$ CANDIDATES

The signal for $\eta \to \pi^0\gamma\gamma$ decay was searched for as a peak in the invariant-mass spectrum of the $\pi^0\gamma\gamma$ final state at

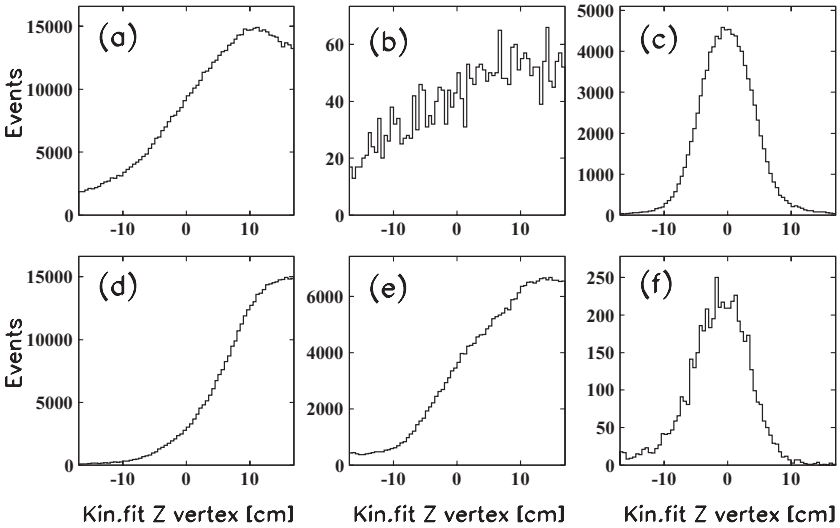

FIG. 2. Distributions of the vertex z coordinate obtained from the kinematic-fit output for the $\pi^- p \to \pi^0\gamma\gamma n \to 4\gamma n$ hypothesis: (a) LH_2 data, (b) empty-target data, (c) MC simulation for $\pi^- p \to \eta n \to \pi^0\gamma\gamma n$, (d) MC for $\pi^- p \to \eta n \to 3\pi^0 n$, (e) MC for $\pi^- p \to \pi^0\pi^0 n$, and (f) MC for $\pi^- p \to \eta n \to \gamma\gamma n$.

the mass region of the η meson. To do that, we had to select candidates for the $\pi^- p \to \pi^0\gamma\gamma n \to 4\gamma n$ process.

The major contribution to the sample with four photons in the final state comes from the direct $\pi^0\pi^0$ production. We have measured the kinematic features of the $\pi^0\pi^0$ production in our energy range and presented them in Ref. [18]. The MC simulation of this process is described in Ref. [14]. Note that the $\pi^0\pi^0$ background does not produce a peak in the η-mass region. However, for a reliable analysis of the $\eta \to \pi^0\gamma\gamma$ signal, the $\pi^- p \to \pi^0\pi^0 n \to 4\gamma n$ events must be separated from the $\pi^0\gamma\gamma$ candidates. The kinematic-fitting technique was used to test the various reaction hypotheses needed in our analysis. The suppression of background processes and the selection of good event candidates was based on the confidence level (CL) of the corresponding fits. The $\pi^0\pi^0$ background was significantly suppressed by discarding all events that satisfied the $\pi^- p \to \pi^0\pi^0 n \to 4\gamma n$ hypothesis with a probability larger than 0.01%. The $\pi^- p \to \pi^0\pi^0 n$ events can also contribute to the four-cluster sample when the neutron is detected and one of the photons escapes detection in the CB. Based on the MC simulation, we conclude that the test of the $\pi^- p \to \pi^0\gamma n \to 3\gamma n$ hypothesis removes most of this background. Therefore, all events that satisfied this hypothesis with a probability larger than 0.01% were discarded as well. The remaining $\pi^0\pi^0$ background is mostly from events that show up in the tails of the invariant-mass resolution, i.e., when the reconstructed invariant mass of two decay photons from one of the two π^0s is very different from the π^0-meson mass.

In the $m(\pi^0\gamma\gamma)$ spectrum, besides the "smooth" background from the $\pi^0\pi^0$ production, there are also contributions from other neutral η decays that can mimic the $\eta \to \pi^0\gamma\gamma$ signal. The $\eta \to 3\pi^0$ decay can produce a four-cluster event when the photon showers overlap in the CB or photons escape through the CB exit tunnel. The $\eta \to \gamma\gamma$ decay contributes to the four-cluster sample by photon showers split off or by low-energy pile-up clusters that survived our TDC-based elimination procedure.

All background processes can be partially suppressed by making a cut on the confidence level for the hypothesis of the process that we are searching for, $\pi^- p \to \pi^0\gamma\gamma n \to 4\gamma n$. The resulting distributions for the kinematic-fit probability obtained for the experimental data and for different MC simulations can be found in Ref. [14]. An inspection of those probability distributions indicates that tightening the cut on the confidence level increases the signal-to-background ratio only in the probability range below 20% and is not enough for sufficient suppression of the background contributions.

Since the length of the LH_2 target was 10 cm, we could improve the angular resolution using the z coordinate of the event vertex as a free parameter in the kinematic fit. For background reactions, the resulting z-coordinate distributions, which are illustrated in Fig. 2 for different experimental and MC-simulated data, do not correspond to the real vertex distribution. Therefore, applying a cut on the z coordinate, which is obtained from the kinematic fit, allows an improvement of the signal-to-background ratio.

As illustrated in Fig. 3, further suppression of the $\eta \to \gamma\gamma$ and $\pi^0\pi^0$ background contributions can be obtained by applying cuts on the $\pi^0\gamma$ invariant mass with respect to the $\pi^0\gamma\gamma$ invariant mass, where the invariant masses are calculated from the kinematic fit to the $\pi^- p \to \pi^0\gamma\gamma n \to 4\gamma n$ hypothesis. Figure 3(a), (b), (c) shows the larger of the two $m(\pi^0\gamma)$ values for $\pi^0\pi^0$, $\eta \to \gamma\gamma$ and $\eta \to \pi^0\gamma\gamma$ events, and Fig. 3(d), (e), (f) shows the smaller. The cut on $m_{\max}(\pi^0\gamma)$ implies discarding all events that lie above the line. Three cuts with different efficiencies are tested; they reject much of the $\pi^0\pi^0$ background, almost all $\eta \to \gamma\gamma$ background, and just a few $\eta \to \pi^0\gamma\gamma$ events. The purpose of testing different cuts is to check the sensitivity of our results to the fraction of the $\pi^0\pi^0$ and $\eta \to \gamma\gamma$ background events left and to changes in the Dalitz plot acceptance. Further tightening the $m_{\max}(\pi^0\gamma)$ cut is not desirable, as it results in cutting off the larger $m(\pi^0\gamma)$ values in the $\eta \to \pi^0\gamma\gamma$ Dalitz plot, which are important for measuring the decay amplitude. The cut on $m_{\min}(\pi^0\gamma)$ requires discarding all events that lie below the line. This cut mostly helps to suppress additionally the $\eta \to \gamma\gamma$ background. Tightening the $m_{\min}(\pi^0\gamma)$ cut is also not desirable, as it results in cutting off the lowest $m(\pi^0\gamma)$

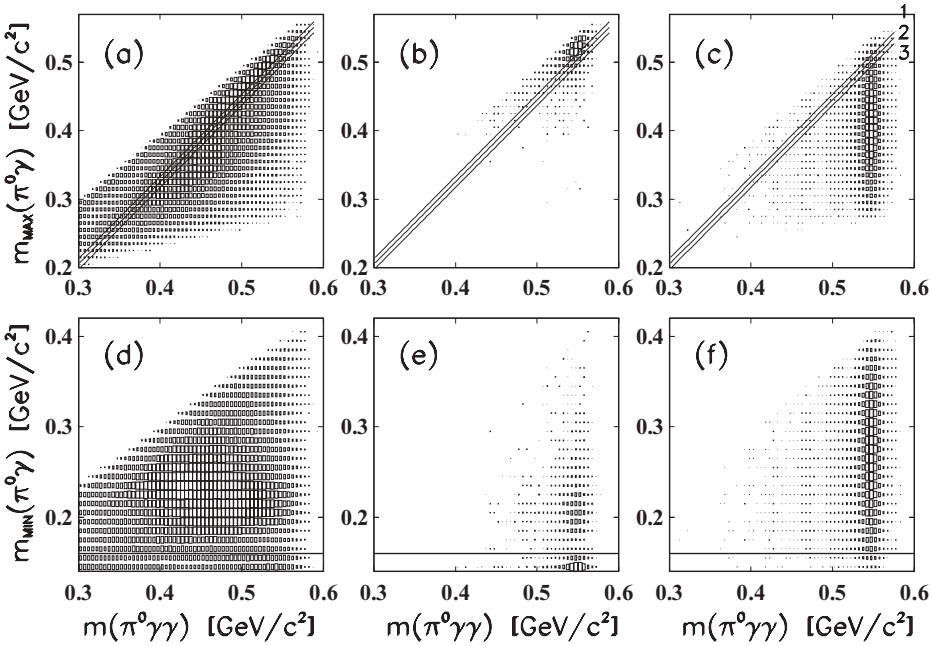

FIG. 3. Two-dimensional density distributions of the larger (top) and smaller (bottom) $\pi^0\gamma$ invariant mass versus the $\pi^0\gamma\gamma$ invariant mass for events selected as $\pi^- p \to \pi^0\gamma\gamma n \to 4\gamma n$ candidates: (a), (d) MC simulation for $\pi^- p \to \pi^0\pi^0 n$, (b), (e) MC for $\pi^- p \to \eta n \to 3\pi^0 n$, (c),(f) MC for $\pi^- p \to \eta n \to \pi^0\gamma\gamma n$. The lines in distributions (a), (b), and (c) depict the three cuts that are tested. These cuts are implemented by discarding all events for which $m_{\max}(\pi^0\gamma)$ lies above the line. The line in distributions (d), (e), and (f) depicts the cut on $m_{\min}(\pi^0\gamma)$. This cut requires discarding all events for which $m_{\min}(\pi^0\gamma)$ lies below the line.

values in the $\eta \to \pi^0\gamma\gamma$ Dalitz plot. The complete elimination of the $\eta \to \gamma\gamma$ background can be achieved by the additional requirement that the energy of each of the four clusters must be larger than 40 MeV. This cut is especially helpful for clearing the $\eta \to \gamma\gamma$ background from low-energy pile-up clusters that survived the TDC-based elimination procedure.

Four-cluster events can also occur by the $\pi^- p \to \pi^0 n \to \gamma\gamma n$ process, in a way similar to the $\eta \to \gamma\gamma$ events. However, events from this background lie much below the η-mass region and can be neglected in the analysis. See Ref. [14] for more details on this background.

Since the $\eta \to 3\pi^0$ background in the η-mass region occurs mostly due to overlapping clusters, those events can be partially eliminated from the events with normal single-photon clusters by testing the cluster radius. The so-called effective radius R of a cluster containing k crystals with energy E_i deposited in crystal i is defined as $R = \sqrt{\sum_i^k E_i \cdot (\Delta r_i)^2 / \sum_i^k E_i}$, where Δr_i is the opening angle (in radians) between the cluster direction and the crystal axis. For events selected as $\pi^- p \to \pi^0\gamma\gamma n \to 4\gamma n$ candidates, we compare in Fig. 4 two-dimensional density distributions of cluster radius R versus cluster energy. Figure 4(a), (b) shows this distribution for the two "direct" (i.e., supposed to be produced directly from the η decay, without coupling to π^0) photons, and Fig. 4(c), (d) shows it for the two photons that are from π^0 decay. Figures 4(a), (c) are for the MC simulation of $\eta \to \pi^0\gamma\gamma$ events, and Figs. 4(b), (d) are for the MC simulation of $\eta \to 3\pi^0$ events. The cluster radii for the $\eta \to 3\pi^0$ background events are systematically larger compared to the ones for $\eta \to \pi^0\gamma\gamma$ events, and the lines in the distributions depict the effective radius cuts that are tested. The cuts are such that they discard all events for which at least one R is above the line. Since there is not much difference between the $\eta \to \pi^0\gamma\gamma$ and $\eta \to 3\pi^0$ distributions for cluster energies below 60 MeV, our cuts are effective only above this cluster energy. Two cuts of different efficiencies are tested. Cut no. 1 suppresses the $\eta \to 3\pi^0$ background by a factor of 4, while the detection efficiency for $\eta \to \pi^0\gamma\gamma$ events decreases by 23%. For cut no.2, these values are 9% and 45%, respectively. In order to prove that there is no systematic difference between

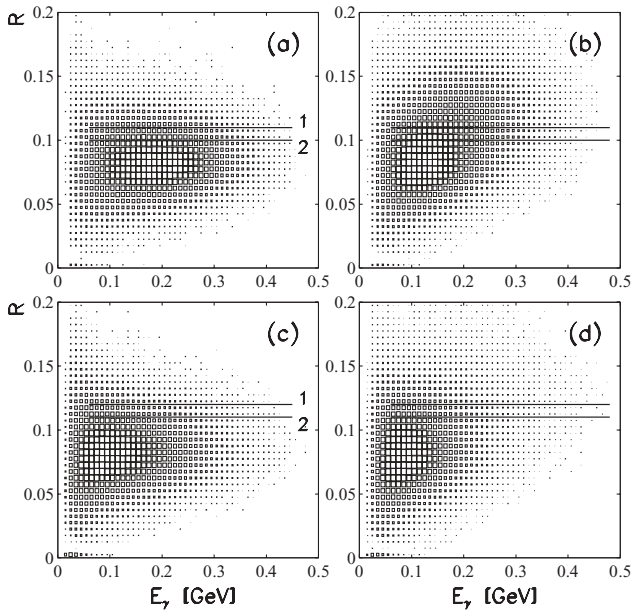

FIG. 4. Two-dimensional density distributions of the effective cluster radius R versus the cluster energy of the photons for events selected as $\pi^- p \to \pi^0\gamma\gamma n \to 4\gamma n$ candidates are shown for the two "direct" photons from η decay (top) and the two photons from the π^0 decay (bottom): (a),(c) MC simulation for $\pi^- p \to \eta n \to \pi^0\gamma\gamma n$, (b),(d) MC for $\pi^- p \to \eta n \to 3\pi^0 n$. The lines in the distributions depict two R-cuts that we tested; they require discarding all events if they have a cluster with energy larger than 0.06 GeV which R lies above the line.

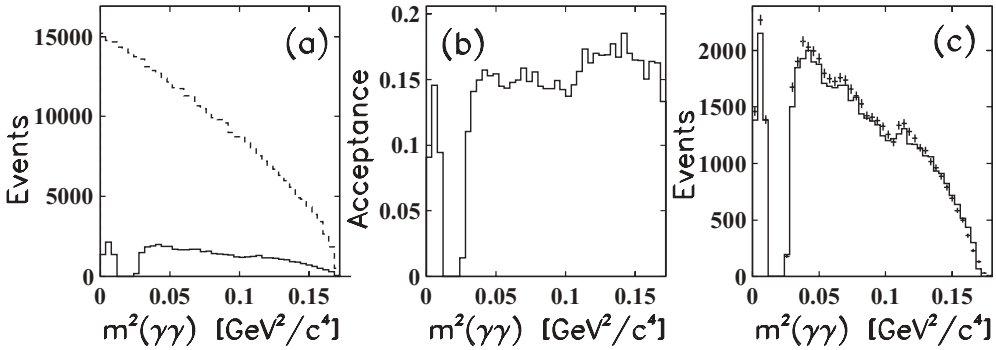

FIG. 5. Spectra that illustrate the $\eta \to \pi^0\gamma\gamma$ acceptance obtained when the events are selected at the 10% CL, with the vertex z coordinate within ± 8 cm, after applying cut no. 1 on the cluster radius R and cut no. 1 on $m_{\max}(\pi^0\gamma)$: (a) $m^2(\gamma\gamma)$ spectrum (dashed line) from 4×10^5 $\pi^- p \to \eta n \to \pi^0\gamma\gamma n$ events, with η decaying according to phase space, which were initially generated as an input to the MC simulation, plus the spectrum (solid line) finally obtained for these events after the MC simulation and analysis; (b) the $\eta \to \pi^0\gamma\gamma$ acceptance as a function of $m^2(\gamma\gamma)$, obtained as the ratio of the two spectra in (a); (c) comparison of the $m^2(\gamma\gamma)$ spectra obtained using the $\pi^- p \to \eta n \to \pi^0\gamma\gamma n \to 4\gamma n$ hypothesis (solid line) and the $\pi^- p \to \pi^0\gamma\gamma n \to 4\gamma n$ hypothesis (crosses).

the effective radius of clusters calculated for the experimental events and for the MC-simulated ones, we compared the R distribution for four clusters of the experimental and MC-simulated events of the $\pi^- p \to \pi^0\pi^0 n \to 4\gamma n$ process. No difference is found. The correctness of our MC simulation for the $\eta \to 3\pi^0$ background can also be illustrated by the agreement of the results obtained with different cuts on R.

All selection criteria are optimized for suppressing the background contributions to the level where the number of the expected $\eta \to \pi^0\gamma\gamma$ events is comparable to the number of background events in the η-mass region. At the same time, we managed to keep a reasonably high detection efficiency for the signal without cutting off much of the $\eta \to \pi^0\gamma\gamma$ Dalitz plot. The acceptance for $\eta \to \pi^0\gamma\gamma$ events is illustrated in Fig. 5 for the case when the event candidates are selected at the 10% CL, with the vertex z coordinate within ± 8 cm, and after applying cut no. 1 on the cluster radius R and cut no. 1 on $m_{\max}(\pi^0\gamma)$. For these selection cuts, the acceptance is about 15% with a hole at the π^0-meson mass. Low and high values of $m(\pi^0\gamma)$ are just slightly cut off in the $\eta \to \pi^0\gamma\gamma$ Dalitz plot. Note good agreement between the $m^2(\gamma\gamma)$ spectra obtained by testing the $\pi^- p \to \eta n \to \pi^0\gamma\gamma n \to 4\gamma n$ and the $\pi^- p \to \pi^0\gamma\gamma n \to 4\gamma n$ hypothesis [see Fig. 5(c)]. This is important, as we are going to use the latter hypothesis for the determination of the experimental $m^2(\gamma\gamma)$ spectrum of the $\eta \to \pi^0\gamma\gamma$ decay.

The last source of background is the empty-target contribution which originates in the pion beam interactions in the target walls or the passage of a μ^- from a π^- decay through the CB. The suppression of this background is described in detail in Ref. [14]. The subtraction of the remaining empty-target background should be made with the weight equal to the ratio of the beam pions incident on the full and the empty target. For this experiment, where few empty-target samples were taken, this ratio is 29.24 : 1. Since the subtraction of a background spectrum with a huge weight factor results in large statistical fluctuations in the remaining distribution, our reanalysis uses a new fitting procedure that avoids this subtraction.

IV. DETERMINATION OF $d\Gamma(\eta \to \pi^0\gamma\gamma)/dm^2(\gamma\gamma)$ AND $BR(\eta \to \pi^0\gamma\gamma)$

Our earlier attempt to measure the $m(\gamma\gamma)$ spectrum for the $\eta \to \pi^0\gamma\gamma$ decay is described in Ref. [14]. The spectrum was obtained by testing the $\pi^- p \to \eta n \to \pi^0\gamma\gamma n \to 4\gamma n$ hypothesis. The selected event candidates also included background events for which the invariant mass of four photons was close to the η mass. Therefore, the resulting distribution still had to be corrected for all remaining backgrounds. That was complicated due to small statistics of the empty-target samples and the limited accuracy in reproducing the $\pi^0\pi^0$ background with the MC simulation. In the present analysis, we solve these problems by using a fitting procedure that is similar to the one that was used earlier for the determination of the $\eta \to \pi^0\gamma\gamma$ branching ratio itself. In this procedure, the $m(\pi^0\gamma\gamma)$ spectrum, which was obtained by testing simply the $\pi^- p \to \pi^0\gamma\gamma n \to 4\gamma n$ hypothesis, was fitted to the $\eta \to \pi^0\gamma\gamma$ signal seen above a smooth background. Similar to that, the determination of the $\eta \to \pi^0\gamma\gamma$ yield as function of $m(\gamma\gamma)$ can be made by repeating this procedure for each individual $m(\gamma\gamma)$ interval. The important feature is that the $\pi^- p \to \pi^0\gamma\gamma n \to 4\gamma n$ hypothesis does not make the resolution in $m(\gamma\gamma)$ much worse in comparison to the kinematic fit with the constraint on the η-meson mass included. In this work, our experimental statistics enables us to divide the data and MC-simulated samples into seven subsamples depending on the $m^2(\gamma\gamma)$ value.

Our old fitting procedure for $m(\pi^0\gamma\gamma)$ spectra, which has been described in Ref. [14], is based on a binned maximum-likelihood technique. In this procedure, the empty-target and MC-simulation spectra are fitted to the experimental spectrum. Similarly to the old determination of the $m(\gamma\gamma)$ spectrum, the major uncertainties of this procedure are due to the low statistics of the empty-target sample and some discrepancy between the real $\pi^0\pi^0$ background and the simulated one. This problem becomes more significant if we want to divide our data into several subsamples. To solve the problem, the experimental spectra of event candidates are first corrected for the $\eta \to \gamma\gamma$ and $\eta \to 3\pi^0$ backgrounds, which can mimic the

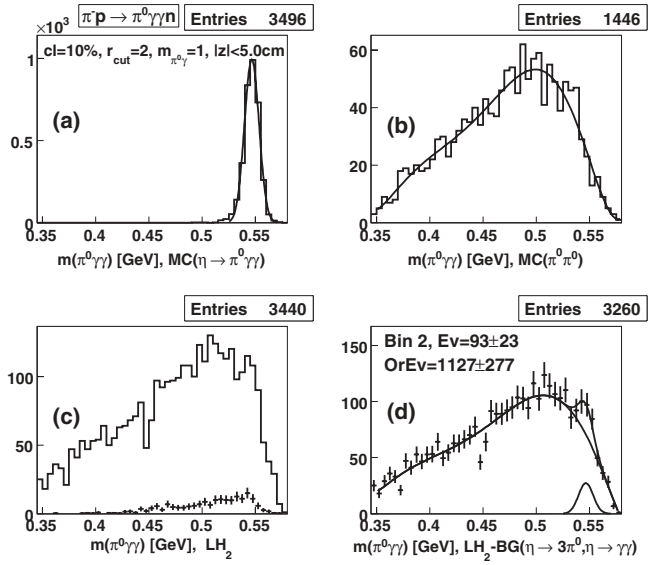

FIG. 6. The $\pi^0\gamma\gamma$ invariant mass spectra for the $\pi^- p \to \pi^0\gamma\gamma n$ candidates selected at the 10% CL, with the vertex z coordinate within ± 5 cm, after applying cut no. 2 on the cluster radius R, cut no. 1 on $m_{\max}(\pi^0\gamma)$, and with $m^2(\gamma\gamma)$ between 0.027 and 0.04 GeV$^2/c^4$: (a) MC simulation for 4×10^5 $\pi^- p \to \eta n \to \pi^0\gamma\gamma n$ events, where the $\eta \to \pi^0\gamma\gamma$ decay is simulated according to phase space; (b) MC for 4×10^7 $\pi^- p \to \pi^0\pi^0 n$ events; (c) experimental LH_2 candidates (solid line) and the $\eta \to 3\pi^0$ background (crosses) expected from the MC simulation; (d) the experimental spectrum remaining after subtraction of the $\eta \to 3\pi^0$ background fitted to a Gaussian for the expected signal plus a polynomial function for the background; the result of the fit to the Gaussian alone is superimposed as well.

signal, and then fitted to a smooth polynomial function for the remaining background with a Gaussian for the expected signal. The initial parameters for the polynomial function are determined from the fit of the MC simulation for the $\pi^0\pi^0$ background; the mean value and sigma for the Gaussian are fixed according to the fit of the MC simulation for the $\eta \to \pi^0\gamma\gamma$ events. This fitting procedure is illustrated in Fig. 6 for the $\pi^- p \to \pi^0\gamma\gamma n$ candidates that are selected at the 10% CL, with the vertex z coordinate within ± 5 cm, and after applying cut no. 2 on the cluster radius R, cut no. 1 on $m_{\max}(\pi^0\gamma)$, and with $m^2(\gamma\gamma)$ between 0.027 and 0.04 GeV$^2/c^4$. The initial number of simulated events in the MC samples shown in Fig. 6 is 4×10^5 for $\pi^- p \to \eta n \to \pi^0\gamma\gamma n$, 4×10^7 for $\pi^- p \to \pi^0\pi^0 n$, and 3×10^7 for $\pi^- p \to \eta n \to 3\pi^0 n$. Prior to the final fitting, the remaining $\eta \to 3\pi^0$ background spectrum is subtracted with a weight factor that is determined from the ratio of the number of the $\eta \to 3\pi^0$ decays observed in this experiment to the number of events generated for this decay in our MC simulation. The same procedure is used for the $\eta \to \gamma\gamma$ background. Usually, after our typical selection cuts, there are few events of the $\eta \to \gamma\gamma$ remaining background left. When the cuts are tight enough, this background becomes negligibly small. Figure 6(d) shows the fit in which the yield of $\eta \to \pi^0\gamma\gamma$ events is determined. The fit results in a signal of 93 ± 23 events, where the error is based on the fit error for the height parameter of the Gaussian. The acceptance for the given $m^2(\gamma\gamma)$ interval and cuts is 8.25%; this implies that 1127 ± 277 $\eta \to \pi^0\gamma\gamma$ events are initially produced.

In order to see the variation of our results for the $\eta \to \pi^0\gamma\gamma$ yield in each $m^2(\gamma\gamma)$ interval, the analysis is repeated several times using different criteria for event selection. The corresponding results for $d\Gamma(\eta \to \pi^0\gamma\gamma)/dm^2(\gamma\gamma)$ in each $m^2(\gamma\gamma)$ interval are listed in Table I. Note that the $m^2(\gamma\gamma)$ interval between 0.011 and 0.027 GeV$^2/c^4$ is absent because of zero acceptance after the suppression of the $\pi^0\pi^0$ background. The acceptance in each $m^2(\gamma\gamma)$ interval is determined using the phase-space simulation of the $\eta \to \pi^0\gamma\gamma$ decay. The decay-width calculation is made by multiplying the $\eta \to \pi^0\gamma\gamma$ branching ratios in each $m^2(\gamma\gamma)$ interval and the full width $\Gamma(\eta \to \text{all}) = 1.29 \pm 0.07$ keV from the latest edition of the Review of Particle Physics [22]. The average results for $d\Gamma(\eta \to \pi^0\gamma\gamma)/dm^2(\gamma\gamma)$ are listed in the last row of Table I. Since the measurements with different selection criteria are correlated, the uncertainties of the average $d\Gamma(\eta \to \pi^0\gamma\gamma)/dm^2(\gamma\gamma)$ values are calculated by adding in quadrature the average of the individual errors in each $m^2(\gamma\gamma)$ interval and the rms of the results themselves. The average results on the dependence of the $\eta \to \pi^0\gamma\gamma$ decay width on $m^2(\gamma\gamma)$ are shown in Fig. 7. In the same Figure, we also depict the χPTh predictions for the $d\Gamma(\eta \to \pi^0\gamma\gamma)/dm^2(\gamma\gamma)$ distribution based on the calculations of Ref. [6]; they have been already illustrated in Fig. 1. The χPTh prediction based on the vector-meson contribution alone seems to match our results better than the other two, where the a_0 contribution is added. A more reliable answer on the $\eta \to \pi^0\gamma\gamma$ decay amplitude, we hope, will be obtained when someone uses our results on $d\Gamma(\eta \to \pi^0\gamma\gamma)/dm^2(\gamma\gamma)$ to fit them to a χPTh-based model.

TABLE I. The $d\Gamma(\eta \to \pi^0\gamma\gamma)/dm^2(\gamma\gamma)$ results (in units [eV/GeV^2]) for seven intervals of $m^2(\gamma\gamma)$ that were obtained using different criteria for event selection. The last row lists the average $d\Gamma(\eta \to \pi^0\gamma\gamma)/dm^2(\gamma\gamma)$ results, which are shown in Fig. 7.

$m^2(\gamma\gamma)$ [GeV$^2/c^4$]	0.–0.011	0.027–0.04	0.04–0.06	0.06–0.08	0.08–0.1	0.1–0.12	0.12–0.17
#1 $d\Gamma/dm^2(\gamma\gamma)$	4.55 ± 1.29	3.05 ± 1.06	2.79 ± 0.59	2.32 ± 0.51	1.96 ± 0.47	1.18 ± 0.47	0.71 ± 0.21
#2 $d\Gamma/dm^2(\gamma\gamma)$	3.82 ± 1.25	2.82 ± 1.04	2.81 ± 0.57	2.01 ± 0.50	1.64 ± 0.45	0.83 ± 0.45	0.61 ± 0.20
#3 $d\Gamma/dm^2(\gamma\gamma)$	4.39 ± 1.07	1.84 ± 0.90	2.47 ± 0.50	1.88 ± 0.48	2.03 ± 0.45	1.66 ± 0.39	0.89 ± 0.19
#4 $d\Gamma/dm^2(\gamma\gamma)$	4.78 ± 1.10	2.88 ± 0.90	2.27 ± 0.50	2.04 ± 0.48	2.04 ± 0.44	1.55 ± 0.39	0.90 ± 0.18
#5 $d\Gamma/dm^2(\gamma\gamma)$	4.92 ± 1.05	2.73 ± 0.89	2.86 ± 0.52	2.14 ± 0.48	2.27 ± 0.45	1.51 ± 0.40	1.02 ± 0.19
#6 $d\Gamma/dm^2(\gamma\gamma)$	4.65 ± 1.21	3.36 ± 0.98	2.27 ± 0.55	2.31 ± 0.50	1.62 ± 0.45	1.05 ± 0.44	0.57 ± 0.20
$\langle\rangle$ $d\Gamma/dm^2(\gamma\gamma)$	4.5 ± 1.2	2.8 ± 1.1	2.58 ± 0.59	2.12 ± 0.51	1.93 ± 0.51	1.30 ± 0.52	0.78 ± 0.25

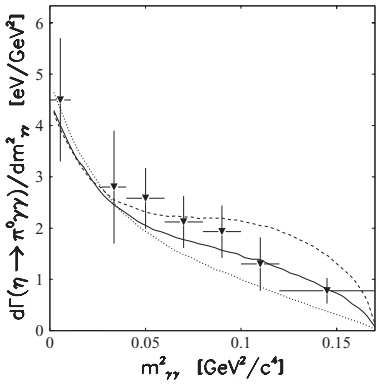

FIG. 7. Our results for $d\Gamma(\eta \to \pi^0\gamma\gamma)/dm^2(\gamma\gamma)$ (triangles) compared to χPTh predictions from Ref. [6]: the vector-meson contribution alone (solid line) and with the a_0 contribution added assuming either the constructive (dash line) or destructive (dot line) interference.

The procedure that is used for obtaining the $d\Gamma(\eta \to \pi^0\gamma\gamma)/dm^2(\gamma\gamma)$ results can also be applied to fitting our full data and MC samples. This procedure is illustrated in Fig. 8 for events selected with the same criteria as the ones used in Fig. 6. The fit results in a signal of 507 ± 54 $\eta \to \pi^0\gamma\gamma$ events and the corresponding branching ratio $(2.38 \pm 0.25) \times 10^{-4}$, or the decay width 0.307 ± 0.032 eV. In order to prove the reliability of our analysis and the correctness of the MC simulations, we checked the sensitivity of our results to the selection criteria used to fill the $m(\pi^0\gamma\gamma)$ spectra. To diminish the uncertainty in the calculation of our overall acceptance depending on the selection criteria applied, the MC simulation of the $\eta \to \pi^0\gamma\gamma$ decays was performed according to the VMD amplitude from Ref. [6]. The number of the $\eta \to \pi^0\gamma\gamma$ events and the corresponding $BR(\eta \to \pi^0\gamma\gamma)$ obtained from the fits with different vertex z-coordinate limits, kinematic-fit CL, cuts on cluster radius R and $m_{\max}(\pi^0\gamma))$ are listed in Table II. The selection cuts corresponding to the result printed with a bold font in Table II are identical to the ones used in the fitting procedure illustrated in Fig. 8. From comparison of these two results, one can see that using the VMD simulation and the phase-space one gives almost the same answer. We explain this agreement by our good acceptance for the full $\eta \to \pi^0\gamma\gamma$ Dalitz plot.

The results compiled in Table II illustrate the stability of our branching ratio values on various tightenings of the selection criteria that improve the signal-to-background ratio, but decrease the number of the $\eta \to \pi^0\gamma\gamma$ events observed. Note that all values for $BR(\eta \to \pi^0\gamma\gamma)$ in Table II overlap within their uncertainties. As our final result for the $\eta \to \pi^0\gamma\gamma$ branching ratio, we take an average of all results listed in Table II, which is 2.21×10^{-4}. The statistical uncertainty is taken from the error of the fit with the largest number of $\eta \to \pi^0\gamma\gamma$ events determined; it is 0.24×10^{-4}. As the first contribution to the systematic uncertainty, we take half the difference between the largest and the smallest value for $BR(\eta \to \pi^0\gamma\gamma)$ in Table II, which is 0.31×10^{-4}. The contribution due to the uncertainty in the background shape under the $\eta \to \pi^0\gamma\gamma$ signal is estimated from the difference between our value for $BR(\eta \to \pi^0\gamma\gamma)$ and the branching ratio estimated from our $d\Gamma(\eta \to \pi^0\gamma\gamma)/dm^2(\gamma\gamma)$ results obtained from the fits of individual intervals of $m^2(\gamma\gamma)$. This difference is about 0.35×10^{-4}. The total systematic uncertainty is calculated by taking these two contributions in quadrature; it gives 0.47×10^{-4}. Then our branching ratio is

$$\begin{aligned} BR(\eta \to \pi^0\gamma\gamma) &= (2.21 \pm 0.24_{\text{stat}} \pm 0.47_{\text{syst}}) \times 10^{-4} \\ &= (2.21 \pm 0.53_{\text{tot}}) \times 10^{-4}. \end{aligned}$$

By using the full width $\Gamma(\eta \to \text{all}) = 1.29 \pm 0.07$ keV from Ref. [22], the partial decay width is

$$\begin{aligned} \Gamma(\eta \to \pi^0\gamma\gamma) &= 0.285 \pm 0.031_{\text{stat}} \pm 0.061_{\text{syst}}\ \text{eV} \\ &= 0.285 \pm 0.068_{\text{tot}}\ \text{eV}. \end{aligned}$$

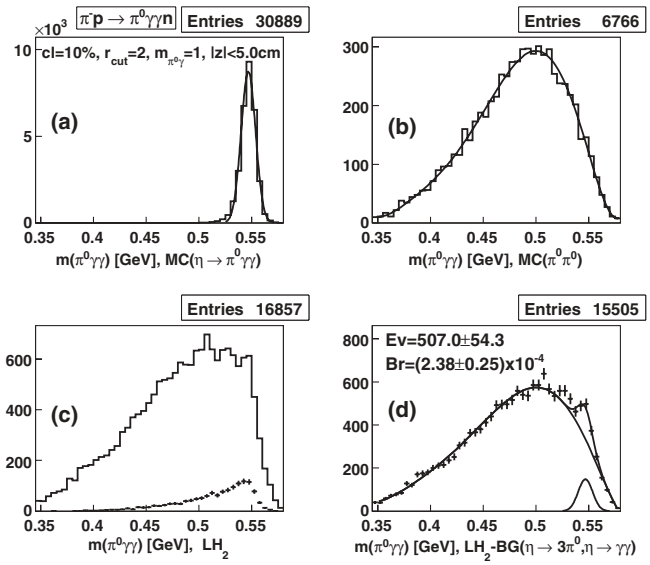

FIG. 8. Same as Fig. 6 but for the full $m^2(\gamma\gamma)$ spectrum.

V. COMPARISON OF THE REVISED ANALYSIS WITH THE EARLIER ONE

Our new value for the $\eta \to \pi^0\gamma\gamma$ decay width, $\Gamma(\eta \to \pi^0\gamma\gamma) = 0.285 \pm 0.068$ eV, is somewhat smaller than 0.45 ± 0.12 eV reported earlier by us in Ref. [14], but the two values overlap within their uncertainties. For the most part, we explain this difference by the uncertainty in the definition of the $\pi^0\pi^0$ background shape under the $\eta \to \pi^0\gamma\gamma$ signal. From the comparison of the earlier analysis with the present one, we have found that a small discrepancy in the shape between the real $\pi^0\pi^0$ background and its MC simulation resulted in some gain of the weight factor for the $\eta \to \pi^0\gamma\gamma$ signal spectrum in our binned maximum-likelihood fits. In the new fitting procedure, we fix only the $\eta \to \pi^0\gamma\gamma$ peak parameters, taking them according to the MC simulation, while the parameters for the $\pi^0\pi^0$ background were free, but initialized from a fit of the $\pi^0\pi^0$ MC simulation. The second reason for a smaller value of the new result is a better understanding of the source of the $\eta \to \gamma\gamma$ background and the optimization of the selection criteria for its complete elimination. Additionally,

TABLE II. Comparison of the number of $\eta \to \pi^0\gamma\gamma$ events and the corresponding $BR(\eta \to \pi^0\gamma\gamma)$ obtained from the fit of the $m(\pi^0\gamma\gamma)$ spectra for different cuts on the vertex z-coordinate, kinematic-fit CL, effective cluster radius R, and $m_{\max}(\pi^0\gamma)$. The selection cuts corresponding to the result printed with a bold font are identical to the ones used in the fitting procedure illustrated in Fig. 8.

# Events($\eta \to \pi^0\gamma\gamma$); BR($\eta \to \pi^0\gamma\gamma$)[$\times 10^4$] for cuts:	$\lvert Z_V\rvert < 8$ cm	$\lvert Z_V\rvert < 7$ cm	$\lvert Z_V\rvert < 6$ cm	$\lvert Z_V\rvert < 5$ cm
5%CL, #1(R), #1($m_{\max}(\pi^0\gamma)$)	$912 \pm 94; 2.38 \pm 0.24$	$816 \pm 88; 2.20 \pm 0.24$	$769 \pm 81; 2.20 \pm 0.23$	$752 \pm 74; 2.38 \pm 0.24$
5%CL, #1(R), #2($m_{\max}(\pi^0\gamma)$)	$930 \pm 92; 2.43 \pm 0.24$	$823 \pm 86; 2.23 \pm 0.23$	$775 \pm 80; 2.22 \pm 0.23$	$757 \pm 73; 2.40 \pm 0.23$
5%CL, #1(R), #3($m_{\max}(\pi^0\gamma)$)	$956 \pm 91; 2.52 \pm 0.24$	$853 \pm 85; 2.32 \pm 0.23$	$794 \pm 79; 2.29 \pm 0.23$	$771 \pm 72; 2.46 \pm 0.23$
5%CL, #2(R), #1($m_{\max}(\pi^0\gamma)$)	$626 \pm 72; 2.32 \pm 0.27$	$552 \pm 68; 2.11 \pm 0.26$	$532 \pm 63; 2.16 \pm 0.25$	$541 \pm 58; 2.42 \pm 0.26$
5%CL, #2(R), #2($m_{\max}(\pi^0\gamma)$)	$628 \pm 71; 2.33 \pm 0.26$	$548 \pm 66; 2.11 \pm 0.26$	$534 \pm 61; 2.18 \pm 0.25$	$545 \pm 56; 2.45 \pm 0.25$
5%CL, #2(R), #3($m_{\max}(\pi^0\gamma)$)	$650 \pm 70; 2.43 \pm 0.26$	$575 \pm 65; 2.22 \pm 0.25$	$549 \pm 61; 2.25 \pm 0.25$	$556 \pm 56; 2.51 \pm 0.25$
10%CL, #1(R), #1($m_{\max}(\pi^0\gamma)$)	$811 \pm 88; 2.23 \pm 0.24$	$731 \pm 83; 2.07 \pm 0.24$	$688 \pm 77; 2.07 \pm 0.23$	$684 \pm 70; 2.28 \pm 0.23$
10%CL, #1(R), #2($m_{\max}(\pi^0\gamma)$)	$835 \pm 87; 2.30 \pm 0.24$	$740 \pm 82; 2.11 \pm 0.23$	$698 \pm 76; 2.11 \pm 0.23$	$693 \pm 69; 2.31 \pm 0.23$
10%CL, #1(R), #3($m_{\max}(\pi^0\gamma)$)	$860 \pm 86; 2.38 \pm 0.24$	$765 \pm 81; 2.19 \pm 0.23$	$714 \pm 75; 2.17 \pm 0.23$	$702 \pm 68; 2.35 \pm 0.23$
10%CL, #2(R), #1($m_{\max}(\pi^0\gamma)$)	$586 \pm 69; 2.28 \pm 0.27$	$513 \pm 64; 2.07 \pm 0.26$	$489 \pm 60; 2.09 \pm 0.25$	$\mathbf{511 \pm 55; 2.41 \pm 0.26}$
10%CL, #2(R), #2($m_{\max}(\pi^0\gamma)$)	$591 \pm 67; 2.31 \pm 0.26$	$512 \pm 63; 2.07 \pm 0.25$	$492 \pm 58; 2.11 \pm 0.25$	$514 \pm 54; 2.43 \pm 0.25$
10%CL, #2(R), #3($m_{\max}(\pi^0\gamma)$)	$612 \pm 66; 2.40 \pm 0.26$	$532 \pm 62; 2.16 \pm 0.25$	$504 \pm 57; 2.17 \pm 0.25$	$478 \pm 53; 2.27 \pm 0.25$
15%CL, #1(R), #1($m_{\max}(\pi^0\gamma)$)	$727 \pm 84; 2.10 \pm 0.24$	$656 \pm 79; 1.96 \pm 0.24$	$627 \pm 74; 1.98 \pm 0.23$	$646 \pm 68; 2.26 \pm 0.24$
15%CL, #1(R), #2($m_{\max}(\pi^0\gamma)$)	$754 \pm 83; 2.18 \pm 0.24$	$670 \pm 78; 2.01 \pm 0.23$	$641 \pm 72; 2.03 \pm 0.23$	$656 \pm 67; 2.30 \pm 0.23$
15%CL, #1(R), #3($m_{\max}(\pi^0\gamma)$)	$777 \pm 82; 2.26 \pm 0.24$	$696 \pm 77; 2.09 \pm 0.23$	$661 \pm 71; 2.11 \pm 0.23$	$667 \pm 66; 2.35 \pm 0.23$
15%CL, #2(R), #1($m_{\max}(\pi^0\gamma)$)	$526 \pm 66; 2.15 \pm 0.27$	$457 \pm 62; 1.93 \pm 0.26$	$436 \pm 57; 1.96 \pm 0.26$	$461 \pm 53; 2.28 \pm 0.26$
15%CL, #2(R), #2($m_{\max}(\pi^0\gamma)$)	$539 \pm 64; 2.21 \pm 0.26$	$463 \pm 60; 1.97 \pm 0.26$	$446 \pm 56; 2.01 \pm 0.25$	$467 \pm 52; 2.32 \pm 0.26$
15%CL, #2(R), #3($m_{\max}(\pi^0\gamma)$)	$561 \pm 64; 2.31 \pm 0.26$	$487 \pm 59; 2.08 \pm 0.25$	$461 \pm 55; 2.09 \pm 0.25$	$476 \pm 51; 2.37 \pm 0.25$
20%CL, #1(R), #1($m_{\max}(\pi^0\gamma)$)	$711 \pm 81; 2.17 \pm 0.25$	$639 \pm 76; 2.02 \pm 0.24$	$612 \pm 71; 2.05 \pm 0.24$	$624 \pm 65; 2.31 \pm 0.24$
20%CL, #1(R), #2($m_{\max}(\pi^0\gamma)$)	$732 \pm 80; 2.24 \pm 0.24$	$648 \pm 75; 2.05 \pm 0.24$	$621 \pm 69; 2.09 \pm 0.23$	$629 \pm 64; 2.33 \pm 0.24$
20%CL, #1(R), #3($m_{\max}(\pi^0\gamma)$)	$762 \pm 79; 2.35 \pm 0.24$	$686 \pm 74; 2.18 \pm 0.24$	$650 \pm 69; 2.20 \pm 0.23$	$650 \pm 63; 2.42 \pm 0.23$
20%CL, #2(R), #1($m_{\max}(\pi^0\gamma)$)	$495 \pm 63; 2.15 \pm 0.27$	$425 \pm 59; 1.90 \pm 0.26$	$412 \pm 55; 1.96 \pm 0.26$	$437 \pm 50; 2.29 \pm 0.26$
20%CL, #2(R), #2($m_{\max}(\pi^0\gamma)$)	$503 \pm 62; 2.19 \pm 0.27$	$426 \pm 58; 1.92 \pm 0.26$	$417 \pm 54; 1.99 \pm 0.26$	$440 \pm 49; 2.31 \pm 0.26$
20%CL, #2(R), #3($m_{\max}(\pi^0\gamma)$)	$532 \pm 61; 2.32 \pm 0.27$	$459 \pm 57; 2.08 \pm 0.26$	$442 \pm 53; 2.12 \pm 0.25$	$458 \pm 49; 2.42 \pm 0.26$

our selection criteria were optimized in order to have a good acceptance for the entire $\eta \to \pi^0\gamma\gamma$ Dalitz plot, which provided good experimental statistics for the full $m(\gamma\gamma)$ range. All these improvements resulted in a better consistency of the $BR(\eta \to \pi^0\gamma\gamma)$ values obtained with different selection criteria (for comparison see Table I in Ref. [14]) and, as a consequence, in smaller uncertainties in the final results.

Using the new fitting procedure to the data subsets from different $m^2(\gamma\gamma)$ intervals allowed for the first time to obtain reliable results on $d\Gamma(\eta \to \pi^0\gamma\gamma)/dm^2(\gamma\gamma)$; that was not achieved in the earlier analysis.

Thus, the results presented in this work supersede our results reported earlier in Refs. [11,12,14].

VI. SUMMARY AND CONCLUSIONS

We have investigated the rare, doubly radiative decay $\eta \to \pi^0\gamma\gamma$ with a revised analysis of existing data of the Crystal Ball experiment at the AGS [14]. The analysis yields the first information on the dependence of the decay width on the two-photon invariant mass squared, $d\Gamma(\eta \to \pi^0\gamma\gamma)/dm^2(\gamma\gamma)$ (see Table I). A re-evaluation of the branching ratio is also made, $BR(\eta \to \pi^0\gamma\gamma) = (2.21 \pm 0.24_{\text{stat}} \pm 0.47_{\text{syst}}) \times 10^{-4}$; it implies that the decay width is $\Gamma(\eta \to \pi^0\gamma\gamma) = 0.285 \pm 0.031_{\text{stat}} \pm 0.061_{\text{syst}}$ eV. These results are close to predictions based on chiral perturbation theory with vector-meson dominance.

ACKNOWLEDGMENTS

This work was supported in part by DOE and NSF of the U.S., NSERC of Canada, the Russian Ministry of Industry, Science and Technologies, and the Russian Foundation for Basic Research. We thank SLAC for the loan of the Crystal Ball. The assistance of BNL and AGS with the setup is much appreciated.

[1] J. Gasser and H. Leutwyler, Nucl. Phys. **B250**, 465 (1985).
[2] M. M. Achasov *et al.* (SND Collaboration), Nucl. Phys. **B600**, 3 (2001).
[3] F. Binon *et al.*, Yad. Fiz. **33**, 1534 (1981); Lett. Nuovo Cimento A **71**, 497 (1982).
[4] D. Alde *et al.*, Z. Phys. C **25**, 225 (1984).
[5] Ll. Ametller, J. Bijnens, A. Bramon, and F. Cornet, Phys. Lett. **B276**, 185 (1992).
[6] J. N. Ng and D. J. Peters, Phys. Rev. D **46**, 5034 (1992).
[7] J. N. Ng and D. J. Peters, Phys. Rev. D **47**, 4939 (1993).
[8] P. Ko, Phys. Rev. D **47**, 3933 (1993).
[9] M. Jetter, Nucl. Phys. **B459**, 283 (1996).

[10] Y. Nemoto, M. Oka, and M. Takizawa, Phys. Rev. D **54**, 6777 (1996).
[11] S. Prakhov (for the Crystal Ball Collaboration), Phys. At. Nucl. **65**, 2238 (2002).
[12] B. M. K. Nefkens and J. W. Price, *Eta Physics Handbook*, [Phys. Scr. **T99**, 114 (2002)].
[13] N. Knecht *et al*., Phys. Lett. **B589**, 14 (2004).
[14] S. Prakhov *et al*. (Crystal Ball Collaboration), Phys. Rev. C **72**, 025201 (2005).
[15] E. Oset, J. R. Pelaez, and L. Roca, Phys. Rev. D **67**, 073013 (2003).
[16] A. E. Radzhabov and M. K. Volkov, Phys. Rev. D **74**, 113001 (2006).
[17] B. Di Micco *et al*. (KLOE Collaboration), Acta Phys. Slov. **56**, 403 (2006).
[18] S. Prakhov *et al*. (Crystal Ball Collaboration), Phys. Rev. C **69**, 045202 (2004).
[19] W. B. Tippens *et al*. (Crystal Ball Collaboration), Phys. Rev. Lett. **87**, 192001 (2001).
[20] A. Starostin *et al*. (Crystal Ball Collaboration), Phys. Rev. C **64**, 055205 (2001).
[21] M. E. Sadler *et al*. (Crystal Ball Collaboration), Phys. Rev. C **69**, 055206 (2004).
[22] A. B. Balantekin *et al*. (Particle Data Group), J. Phys. G: Nucl. Part. Phys. **33**, 1 (2006).